Turkish Journal of Physics

http://journals.tubitak.gov.tr/physics/

Research Article

Turk J Phys
(2016) 40: 219 – 230

doi:10.3906/fiz-1511-13

A comparative study of the electronic properties of aluminum nitride compounds

Rezek MOHAMMAD[1], **Şenay KATIRCIOĞLU**[2,*]
[1]Department of Applied Physics, Palestine Technical University-Khadoorie, Tulkarem, West Bank, Palestine
[2]Department of Physics, Middle East Technical University, Ankara, Turkey

Received: 24.11.2015 • **Accepted/Published Online:** 15.03.2016 • **Final Version:** 01.12.2016

Abstract: Electronic properties of aluminum nitride in wurtzite, zinc-blende, and rock-salt phases are investigated by a full potential-linearized augmented plane waves method based on density functional theory within standard local density approximation and its four improved versions. Local density approximation corrected by the generalized gradient functional of Perdew–Wang–Engel–Vosko is found to be more successful than the other generalized gradient functional approximations considered in this work for providing reasonable lattice constants, energy gaps, effective electron and hole masses, and optical features for AlN phases. Although local density approximation corrected by modified Becke–Johnson potential underestimates the static dielectric constants, it provides the largest energy gaps of AlN phases very close to the available experimental and theoretical ones reported by high-cost calculations in the literature. Hence, this approach is decided to be the most accurate scheme among other approximations of this work for electronic band structure calculations of aluminum nitride phases.

Key words: Aluminum nitride, full potential-linearized augmented plane waves, density functional theory, electronic properties

1. Introduction

Aluminum nitride (AlN) with a wide band gap ($\approx$6 eV [1,2] in wurtzite (WZ), 5.34 eV [3] in zinc-blende (ZB)) and high electrical resistivity ($\geq 10^{12}\,\Omega$-cm) [4] is a promising candidate material for applications in optoelectronic devices [5–7]. Particularly, AlN has great potential for light emitting diodes (LEDs), laser diodes (LDs), and optical detectors. AlN is also an important interlayer material to improve the electrical and photovoltaic properties of InGaN- and Si-based solar cells [8,9]. A thin AlN layer inserted between the main layers of InGaN/p-InGaN single junction solar cells suppresses the structural defects and reduces the leakage current both in the reverse and forward bias [8]. The nano structure of AlN was reported to be an excellent interlayer for Si-based double junction solar cells (Si/n – InGaN/p – InGaN), exhibiting better quantum efficiency and performance compared to SiO_2 and SiN_4 interlayers [9]. AlN was also presented to be a better capping layer as an antireflective coating than the currently used aluminum oxide on solar cell emitters [10].

AlN in hexagonal WZ (or B4) crystal structur has been reported to be a stable phase with the lattice constant of 3.11 Å (c$\simeq$ 4.98 Å) [1,11,12]. It has been also reported that AlN can crystallize in metastable ZB (or B3) [3,13–15] and rock-salt (RS or B1) [16–18] structures with the lattice constants of $\sim$4.4 Å and $\sim$4.04 Å, respectively, under certain experimental conditions.

*Correspondence: senay@metu.edu.tr

The theoretical works done so far on AlN have mainly tried to verify the structural features measured for the stable WZ and metastable ZB and RS phases. Some of the works among them have also calculated the electronic band structures of AlN in the WZ [19–29], ZB [20–23,25–27,29–31] and RS [19,28,29] phases. Although most of these works have given lattice constants and bulk moduli very close to the measured ones, they could not calculate the respective energy gaps of AlN structures with the same achievement. It was found that the first-principles calculations either by linear muffin-tin orbital [31], pseudopotential [19–23,25,30], or full potential (FP) [27–29,32,33] methods within local density approximation (LDA) or generalized gradient approximation (GGA) of exchange and correlation energies have successfully produced the structural quantities of AlN structures. However, minimum energy gaps between the conduction and valance bands of AlN in WZ and ZB structures very close to the measured ones have been obtained only by quasiparticle and atomic spheres-screened exchange (ASA-SX) corrections on LDA (LDA+QP [20,27,31] and ASA-LDA+SX [24]) involving costly calculations compared to the standard calculations of LDA and GGA. In two recent works [34,35], an energy gap of AlN in the WZ phase close to the measured one was also obtained by modified Becke–Johnson exchange and correlation potential (MBJP) that was designed to reproduce the shape of atomic optimum effective potentials (OEPs) well within either LDA or GGA optimization calculations.

To our knowledge, there is a limited number of works in the literature for the electronic properties of AlN phases extended to optical properties [29, 36, 37]. Among them, only in the work of Reference [29] the optical features of all three AlN phases have been calculated by standard GGA scheme and connected with the corresponding electronic structures.

In the present work, we have examined an approach for the exchange and correlation energies producing electronic features of three AlN phases comparable with the measured ones. Density functional theory (DFT) calculations have carried out for three structures of AlN within standard LDA and three GGA schemes. The electronic band structures of AlN phases presently calculated within the LDA scheme have been also improved by modified Becke–Johnson exchange and correlation functional used in OEP calculations. We present a comparative study for the energy gaps and the effective masses of electrons and holes in AlN structures. We also present a study for the dielectric functions, absorption spectra, and refractivity functions of AlN phases.

2. Method of calculations

The electronic properties of AlN in WZ (WZ-AlN), ZB (ZB-AlN), and RS (RS-AlN) phases are investigated by self-consistent full potential-linearized augmented plane waves (FP-LAPW) provided in the WIEN2k package [38]. The present electronic band structure calculations are based on our recent work [39], in which the structural properties of AlN in WZ, ZB, and RS phases were studied by eight different approaches of exchange and correlation energies. A detailed explanation about the definitions and the optimizations of the unit cells of the AlN phases was introduced in that work [39] together with the parameters necessary in the FP-LAPW calculations. Among the approximations considered [39], the most accurate scheme and the following one are found as PW-EV-GGA and PBE-GGA, respectively, providing the structural features of AlN phases reflecting the experimental results. Consequently, these two approaches are primarily chosen for the present electronic band structure calculations of the AlN phases. The PW-EV-GGA approach is based on the exchange and correlation energies of LDA [40] corrected by the GGA of Engel and Vosko (EV) [41] and the GGA of Perdew and Wang (PW) [42], respectively. In PBE-GGA, both exchange and correlation energies of LDA [40] are improved by the GGA of Perdew–Burke–Ernzerhof (PBE) [43]. Since PW-EV-GGA and PBE-GGA are the improved schemes of EV-GGA and LDA, the electronic band structures of AlN phases are also calculated by

EV-GGA and LDA, for comparison. Considering the serious improvement of the energy gap of the MBJP scheme reported in the literature for compound semiconductors [34,35], the electronic band structures of AlN phases calculated by LDA are also corrected in this work by MBJP within the OEP method. In the calculations of this scheme, the electron density, gradient of electron density, and kinetic energy density functional of exact exchange potential proposed by Becke and Johnson [44] are modified to yield band gaps comparable to those of the high-cost calculations given in the literature [20,24,27,31]. The electronic band structure calculations within MBJP are performed by FP-LAPW and the local orbitals (FP-LAPW+lo) method implemented in WIEN2k [38].

The electronic band structures of AlN in WZ, ZB, and RS phases are calculated by using the corresponding wave functions of the approximations obtained by self-consistent total energy calculations. The positions and values of the energy gaps are precisely determined by using 21 × 21 × 21 grids corresponding to 484 k points in the irreducible wedge of the Brillouin zone for all AlN phases. It is considered that the PW-EV-GGA, EV-GGA, and MBJP schemes used in this work can provide significant correction for the energy gaps of AlN phases over the LDA and PBE-GGA functional, since the parameters of EV-GGA and MBJP are determined by fitting exact exchange OEP.

In this work, the optical features connected with the energy gaps of the AlN phases are calculated by describing the electron transitions between the occupied and unoccupied electronic ground states presented within the PW-EV-GGA and MBJP schemes. The complex dielectric function ($\varepsilon(\omega) = \varepsilon_1(\omega) + i\varepsilon_2(\omega)$), absorption spectrum, and refractive index resulting from these transitions are calculated for a wide photon energy range by the Kramers–Krőnig relations provided in WIEN2k [38].

3. Results and discussion

The self-consistent total energy calculations reported in [39] are repeated by the approximations of this work and the corresponding optimized unit cells of the AlN phases are acquired. AlN in a WZ structure is optimized by LDA, PBE-GGA, PW-EV-GGA, and EV-GGA schemes with the lattice constants of 3.096 (c = 4.966 Å), 3.139 (c = 5.051 Å), 3.137 (c = 5.044 Å), and 3.246 Å (c = 5.259 Å), respectively. The optimized lattice constants of ZB-AlN by the same approximations are respectively 4.346, 4.405, 4.402, and 4.557 Å. The lattice constant of RS-AlN is found to be 4.013 and 4.208 Å by LDA and EV-GGA schemes. As reported in [39], RS-AlN is optimized with the lattice constant of 4.072 Å by both PBE-GGA and PW-EV-GGA. The lattice constants of AlN phases calculated by PW-EV-GGA and PBE-GGA are found more successful than those of the other approximations considered in [39] for providing values of structural features closest to available experimental ones. The electronic band structures of AlN in optimized WZ, ZB, and RS structures are calculated along different $\vec{k}$ directions within LDA, PBE-GGA, PW-EV-GGA, and EV-GGA schemes. The energy gaps of WZ-AlN corresponding to different symmetry points of the Brillouin zone are tabulated in Table 1, along with the available measured and calculated energy gaps of the other works, for comparison. The electronic band structure calculations of the WZ-AlN phase have given the top of the valence band at the Γ point. According to the present LDA, PBE-GGA, PW-EV-GGA, and EV-GGA calculations, WZ has a large direct energy gap at the Γ point, as was reported in the literature. However, the direct energy gaps presently calculated for WZ-AlN by the LDA, PBE-GGA, and EV-GGA schemes and reported in [19–29] are all found much smaller than the corresponding measured value of ∼6 eV [1,2]. The difference is around 1.5–3 eV. The direct energy gap of WZ-AlN calculated by LDA is found higher than that calculated by PBE-GGA. The lattice constants of WZ-AlN

calculated by LDA and PBE-GGA with a very small difference are both very close to the experimental results [1,11,12]. The small decrease of the lattice constant in the experimental value side by LDA calculations causes more separation between the conduction and valance bands. This relation between the energy gaps of LDA and PBE-GGA calculations was also reported in [25] (Table 1). The difference between the experimental direct energy gap of WZ-AlN and the calculated one is decreased to $\sim$1 eV when the exchange-correlation energies are defined by the PW-EV-GGA functional. The direct gap of 5.04 eV (Table 1) calculated for WZ-AlN by the present low-cost PW-EV-GGA calculations is higher than those reported by the standard LDA and GGA calculations [20–23,25,27–29]. Furthermore, this value of the direct energy band gap is found close to the value of high-cost quasiparticle calculations [20]. Therefore, the PW-EV-GGA scheme is determined to be effective to produce a larger direct gap for the WZ-AlN. The electronic band structure of WZ-AlN presently calculated by the PW-EV-GGA scheme is plotted in Figure 1. The PW-EV-GGA scheme does not alter the main band structure of WZ-AlN given commonly by LDA, PBE-GGA, and EV-GGA schemes, but the magnitude of the fundamental energy gap is enlarged by $\sim$0.6–1.3 eV. The present energy gaps calculated by PW-EV-GGA at K, M, and A symmetry points with respect to the Γ point ($E_g^{\Gamma\rightarrow K}$, $E_g^{\Gamma\rightarrow M}$, $E_g^{\Gamma\rightarrow A}$) are also found to be larger than the ones obtained by the present LDA, PBE-GGA, and EV-GGA calculations (Table 1) and LDA calculations given in [19,20,24]. The largest direct transition energy from the valence band to conduction band at the M point is calculated to be 7.40 eV (Table 1) by the PW-EV-GGA scheme with respect to the value of 6.2 eV reported by standard LDA calculations in [20]. The difference between the present transition energy and the ones reported by high-cost LDA+QP [20, 27] and ASA-LDA+SX [24] calculations is $\sim$1 eV.

Table 1. The calculated and measured energy band gaps (E_g (eV)) of AlN in WZ structure.

Ref.	Approach	$E_g^{\Gamma\rightarrow\Gamma}$	$E_g^{\Gamma\rightarrow K}$	$E_g^{\Gamma\rightarrow M}$	$E_g^{\Gamma\rightarrow A}$	$E_g^{M^v\rightarrow M^c}$
[PW]	LDA	4.32	4.91	5.71	6.52	6.59
[PW]	PBE-GGA	3.96	5.05	5.74	6.24	6.27
[PW]	PW-EV-GGA	5.04	6.18	6.72	7.24	7.40
[PW]	EV-GGA	3.77	6.07	6.34	6.07	5.82
[19]	LDA	3.09	4.36	4.93	5.57	
[20]	LDA	3.9	4.8	5.5	6.1	6.2
[20]	LDA+QP	5.8	6.7	7.4	8.3	8.3
[21]	LDA	4.41				
[22]	LDA	4.56				
[23]	LDA	4.44				
[24]	ASA-LDA	4.6	5.5	5.9	6.6	6.6
[24]	ASA-LDA+SX	6.3	7.4	8.1	8.6	8.7
[25]	LDA	4.74				
[25]	GGA	4.245				
[26]	HF-GGA	5.25				
[27]	LDA	4.2				
[27]	LDA+QP	6.05				8.18
[28]	LDA	4.13				
[29]	GGA	4.26	5.16	5.94	6.39	
[1] [2]	Exp. Exp.	6.28 6.12				

[PW]: Present work.

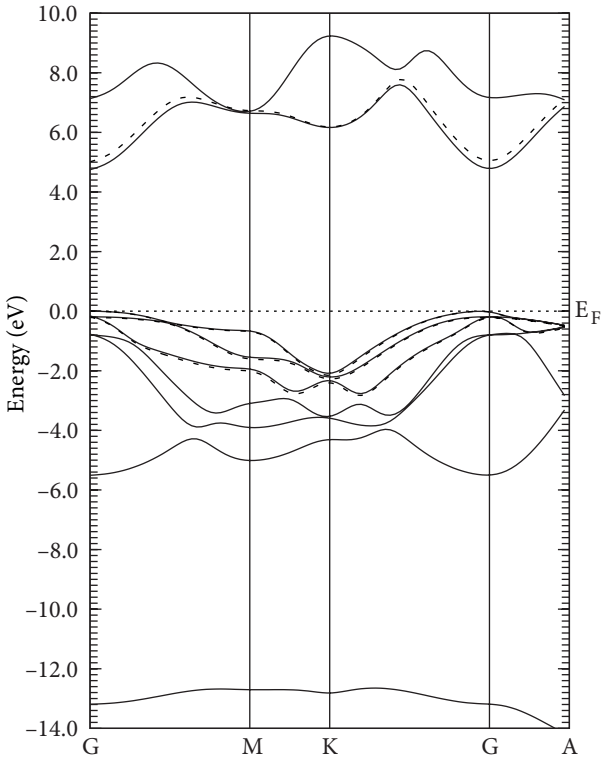

Figure 1. The electronic band structure of WZ-AlN within PW-EV-GGA. The dotted lines show the correction by MBJP calculations.

The electronic band structures of the ZB-AlN and RS-AlN phases calculated within the PW-EV-GGA scheme are plotted in Figures 2 and 3. These figures display that both structures are indirect band gap semiconductors with an energy gap at the X symmetry point. The main energy gaps of the ZB-AlN and RS-AlN structures are tabulated in Tables 2 and 3. Since the optimized lattice constant of ZB-AlN calculated by PB-GGA is closer to the experimental ones [3,13–15] than that calculated by LDA, PBE-GGA gives a larger indirect energy gap for ZB-AlN than LDA. The lattice constant of LDA being closer to the experimental values [16–18] than that of PBE-GGA makes the indirect band gap of RS-AlN wider. It is found that PW-EV-GGA has given the largest indirect energy gap for both ZB-AlN and RS-AlN structures (Tables 2 and 3) among the other exchange-correlation energy approximations considered in this work (LDA, PBE-GGA, EV-GGA). The indirect energy gap of ZB-AlN presently calculated by the PW-EV-GGA scheme is also greater than the ones calculated within LDA by other works [20,24,27,29,31], except the indirect gaps of LDA corrected by high-cost QP [20,27,31] and SX approximation calculations [24] (Table 2). The present indirect gap of 4.22 eV obtained for the ZB-AlN structure within the PW-EV-GGA scheme is very close to the measured value of 4.37 eV [45]. However, it is found small with respect to the corresponding result (5.34 eV) [3] of extinction coefficient data by an amount $\sim$1 eV. Although the direct band gap transition energy of ZB-AlN at the Γ symmetry point is enlarged to 4.74 eV by the present PW-EV-GGA calculations, it is still small compared to the corresponding results of LDA corrected by QP [20,27] and SX [24] approximations (Table 2). The electronic band structure of RS-AlN calculated within PW-EV-GGA (Figure 3) compared well with those reported in [19,28,29]. However, citing first the indirect energy gap of RS-AlN at the X symmetry point, all the energy gaps at Γ, K, and L symmetry points are larger than the ones given by LDA [19] and GGA calculations [29].

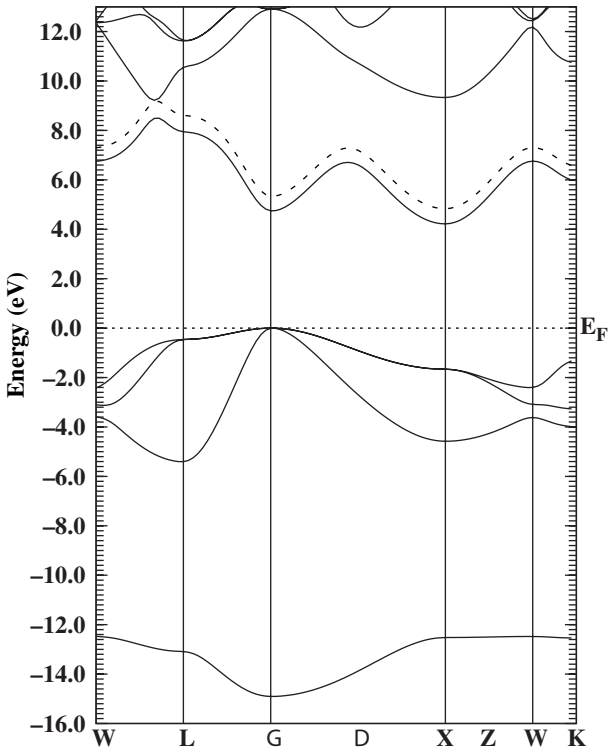

Figure 2. The electronic band structure of ZB-AlN within PW-EV-GGA. The dotted lines show the correction by MBJP calculations.

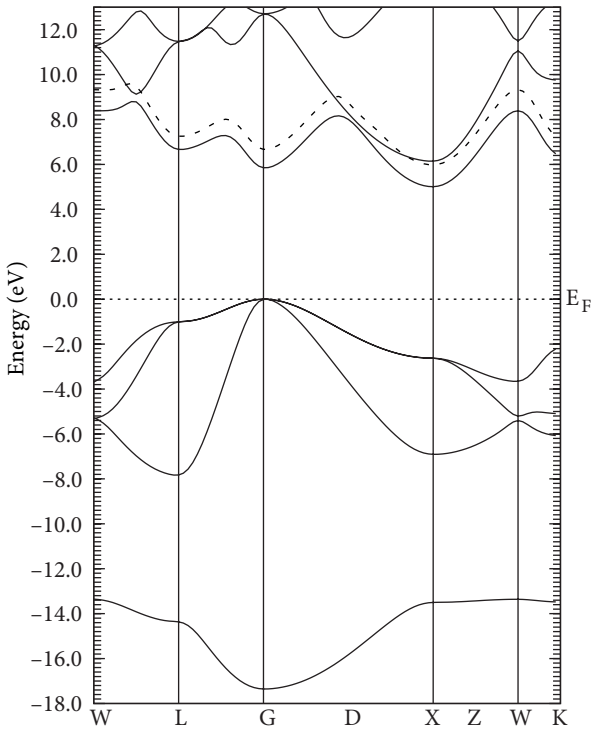

Figure 3. The electronic band structure of RS-AlN within PW-EV-GGA. The dotted lines show the correction by MBJP calculations.

In the present work, the electronic band structures of AlN in WZ, ZB, and RS phases are also reproduced by MBJP within LDA calculations. The improvements of the band structures of WZ-AlN, ZB-AlN, and RS-AlN by MBJP calculations are shown in the plots of Figures 1–3. The band structures are found to be mainly not changed, but the energy gaps of the phases are enlarged by MBJP calculations. The direct and indirect energy gaps for WZ-AlN and ZB-AlN are presently calculated to be 5.61 and 4.83 eV, respectively, by the MBJP scheme. The direct band gap of WZ-AlN was reported to be 5.56 eV [35] in a recent work by similar MBJP calculations. The direct and indirect energy gaps of WZ-AlN and ZB-AlN newly calculated by MBJP are close to the corresponding values of LDA corrected by QP [20] and SX [24] approximations (Tables 1 and 2). The energy gaps of WZ-AlN and ZB-AlN at X ($E_g^{\Gamma\to X}$) and Γ ($E_g^{\Gamma\to\Gamma}$) are also enlarged to 7.32 and 5.33 eV, respectively, within the present MBJP calculations. The respective energy gaps of RS-AlN at X ($E_g^{\Gamma\to X}$) and Γ ($E_g^{\Gamma\to\Gamma}$) points are found to be 5.98 and 6.66 eV by the MBJP scheme.

In this work, the effective electron (m_e^*) and hole (heavy (m_{hh}^*) and light (m_{lh}^*)) masses in the WZ-AlN structure are calculated using the electronic band structures obtained by both the PW-EV-GGA and MBJP schemes (Figure 1). The effective masses are calculated around the minimum of the conduction band (Γ_1^c) and the top of the valence band (Γ_{15}^v) by fitting a quadratic function to the corresponding band structure energies. The present effective electron and hole masses obtained for closely spaced k points along perpendicular (k_x, k_y) and parallel (k_z) directions are tabulated in Table 4 along with the effective masses reported in the literature. The small difference between the corresponding effective masses along the same direction respects the small difference between the present electronic band structure results of the PW-EV-GGA and MBJP schemes around

Table 2. The calculated and measured energy band gaps (E_g (eV)) of AlN in ZB structure.

Ref.	Approach	$E_g^{\Gamma\to\Gamma}$	$E_g^{\Gamma\to X}$	$E_g^{\Gamma\to K}$	$E_g^{\Gamma\to L}$	$E_g^{X^v\to X^c}$
[PW]	LDA	4.36	3.24	5.10	7.40	5.05
[PW]	PBE-GGA	3.98	3.31	5.12	7.15	5.06
[PW]	PW-EV-GGA	4.74	4.22	5.97	7.94	5.88
[PW]	EV-GGA	3.85	4.16	5.76	6.97	5.72
[20]	LDA	4.2	3.2		7.3	
[20]	LDA+QP	6.0	4.9		9.3	
[21]	LDA	4.35				
[22]	LDA	4.50				
[23]	LDA	4.09				
[24]	ASA-LDA	4.2	3.2		7.3	
[24]	ASA-LDA+SX	6.5	5.7		9.8	
[25]	LDA	4.75				
[25]	GGA	4.13				
[26]	HF-GGA		4.26			
[27]	LDA		3.24			
[27]	LDA+QP	6.17	5.11			6.89
[29]	LDA		4.754			
[29]	GGA	4.09	3.38		7.28	
[30]	LDA		4.754			
[31]	LDA		3.47		9.15	
[31]	LDA+QP	5.84	5.11			
[3]	Exp.		5.34			
[45]	Exp.		4.37			

[PW]: Present work.

Table 3. The calculated energy band gaps (E_g (eV)) of AlN in RS structure.

Ref.	Approach	$E_g^{\Gamma\to\Gamma}$	$E_g^{\Gamma\to X}$	$E_{\mathbf{g}}^{\mathbf{\Gamma}\to K}$	$E_g^{\Gamma\to L}$	$E_g^{X^v\to X^c}$
[PW]	LDA	6.08	4.67	5.87	6.27	7.54
[PW]	PBE-GGA	5.40	4.43	5.74	6.02	7.17
[PW]	PW-EV-GGA	5.84	5.01	6.39	6.67	7.64
[PW]	EV-GGA	4.50	4.06	5.65	6.06	6.45
[19]	LDA	4.99	4.04		5.52	
[28]	LDA		4.92			
[29]	GGA	5.42	4.47	5.75	6.18	7.0

[PW]: Present work.

the Γ point (Figure 1). The electron and hole (heavy and light) effective masses presently calculated in WZ-AlN are in the ranges of the corresponding results calculated by other theoretical works [46–50]. It is found that the present electron and hole effective masses are very close to the values calculated by the parameters of effective mass Hamiltonian reproducing the first-principles energy band structures of WZ-AlN near the Γ point [46].

In the present work, the real and imaginary parts of dielectric function ($\varepsilon_1(\omega)$ and $\varepsilon_2(\omega)$) for polarization in the xy plane ($\varepsilon_{1,xy}(\omega)$ and $\varepsilon_{2,xy}(\omega)$) and z direction ($\varepsilon_{1,z}(\omega)$ and $\varepsilon_{2,z}(\omega)$) are calculated for the AlN phases within PW-EV-GGA and plotted in Figure 4. As is observed in Figure 4a, there is a noticeable anisotropy between the dielectric function of WZ-AlN calculated for the polarization in the xy plane and z direction. Since

Table 4. The effective electron and hole masses in WZ-AlN.

	Present work: PW-EV-GGA	MBJP	Other theoretical works:
$m^*_{e,\perp}$ $\Gamma \rightarrow k_x k_y$	0.2567	0.2682	0.25[46], 0.18[47],0.3433[48], 0.30[49],0.32[49],0.27[50]
$m^*_{e,\|\|}$ $\Gamma \rightarrow k_z$	0.3212	0.3381	0.33[46],0.27[47], 0.2938[48],0.29[49],0.30[49],0.28[50]
$m^*_{hh,\perp}$ $\Gamma \rightarrow k_x k_y$	3.1168	3.1171	3.68[46],2.08[47],1.5981[48],4.46[49],4.50[49],2.68[50]
$m^*_{hh,\|\|}$ $\Gamma \rightarrow k_z$	3.6748	3.7640	3.68[46],2.04[47],0.2437[48],0.25[49],1.96[50]
$m^*_{lh,\perp}$ $\Gamma \rightarrow k_x k_y$	0.2669	0.2844	0.25[46],0.20[47],1.4238[48],0.61[49],0.66[49],0.26[50]
$m^*_{lh,\|\|}$ $\Gamma \rightarrow k_z$	0.2769	0.2957	0.25[46],2.04[47],1.4235[48]

the dielectric function for polarization in the xy plane and z direction is isotropic for ZB-AlN and RS-AlN, only $\varepsilon_{1,z}(\omega)$ and $\varepsilon_{2,z}(\omega)$ are plotted in Figures 4b and 4c. The threshold photon energy value of $\varepsilon_2(\omega)$ ($\varepsilon_{2,z}(\omega)$ or $\varepsilon_{2,xy}(\omega)$) at $\sim$5 eV in Figure 4a gives the direct energy gap of WZ-AlN. Similarly, the threshold photon energies of $\varepsilon_{2,z}(\omega)$ found at $\sim$4.2 and 5 eV in Figures 4b and 4c correspond to the indirect band gap energies of ZB-AlN and RS-AlN at the X symmetry point, respectively. The direct and indirect energy gaps of 5.04, 4.22, and 5.01 eV (Tables 1–3) calculated for WZ-AlN, ZB-AlN, and RS-AlN respectively by PW-EV-GGA are also found from the threshold photon energies of absorption functions plotted in Figures 5a–5c. The threshold photon energies of ε_2 (ω) are respectively found at about 5.6, 4.8, and 6 eV within the present MBJP calculations for WZ-AlN, ZB-AlN, and RS-AlN. The first two peaks of $\varepsilon_2(\omega)$ observed in the photon energy ranges from 9 to 13 eV and from 7 to 11 eV for ZB-AlN, RS-AlN, and WZ-AlN (Figures 4a–4c) were associated with the transitions of N 2p electrons into the Al 3p conduction band and N 2p electrons into Al 3p and 2s conduction bands in [29] by partial density of states calculations. Since the energy gaps of AlN phases presently calculated by PW-EV-GGA are wider than the corresponding ones reported in [29] (Tables 1–3), the transition energies given in that work are shifted to higher values in our work. The static dielectric constants of WZ-AlN, $\varepsilon_{1,xy}(0)$ and $\varepsilon_{1,z}(0)$, calculated from the low energy limit values of $\varepsilon_{1,xy}(\omega)$ and $\varepsilon_{1,z}(\omega)$ are 4.09 and 4.29 (Figure 4a). The static dielectric constants are calculated to be 3.81 and 4.88 for ZB-AlN and RS-AlN, respectively (Figures 4b and 4c). The static dielectric constants of AlN phases are also found from the low energy limit value of the refractive index function (n(ω)) plotted in Figures 5d and 5f by the $\varepsilon_1(0) = \mathrm{n}(0)^2$ relation. The static dielectric constants, $\varepsilon_{1,xy}(0)$ and $\varepsilon_{1,z}(0)$, presented in this work for WZ-AlN are comparable to the values of 4.05(4.19) [37], 4.39(4.59) [29], and 4.38(4.61) [36] reported in the literature by GGA and LDA schemes, respectively. While $\varepsilon_{1,z}(0)$ of RS-AlN is comparable with the single available value of 5.13 [29], $\varepsilon_{1,z}(0)$ of ZB-AlN is found small compared to the calculated values of 4.63 [29] and 4.61 [37] and the measured value of 4.68 [51]. On the other hand, the static dielectric constants, 3.65(3.84), 3.76, and 4.35, calculated by MBJP for WZ-AlN, ZB-AlN, and RS-AlN, respectively, are found smaller than those calculated by PW-EV-GGA.

4. Summary and conclusion

FP-LAPW calculations based on DFT within LDA, PBE-GGA, PW-EV-GGA, EV-GGA, and MBJP schemes are introduced for the electronic properties of AlN in WZ, ZB, and RS phases. Local density approximation corrected by the generalized gradient functional of PW-EV-GGA is found more successful than the other generalized gradient functional approximations considered in this work for providing reasonable lattice constants, energy gaps, effective electron and hole masses, and optical features for AlN phases. Although the MBJP scheme underestimates the static dielectric constants, it provides the largest energy gaps of AlN phases very close to

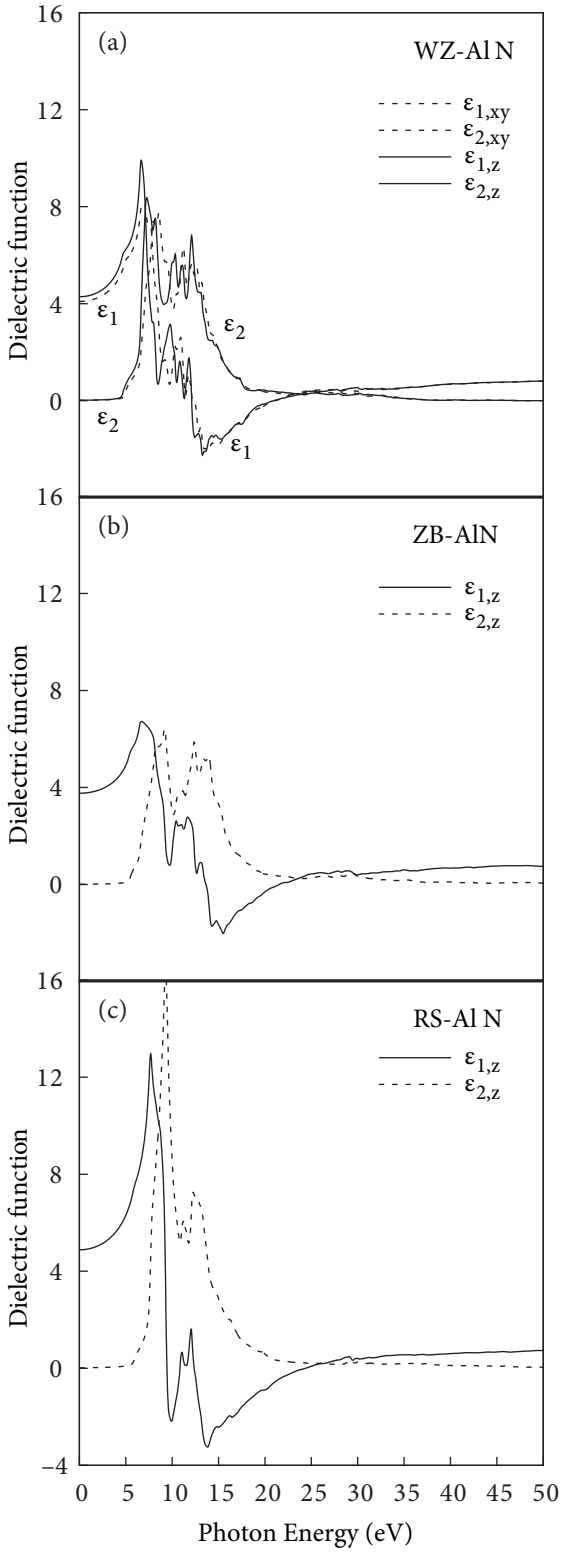

Figure 4. Real and imaginary parts of dielectric function calculated by PW-EV-GGA for WZ-AlN (a), ZB-AlN (b), and RS-AlN (c).

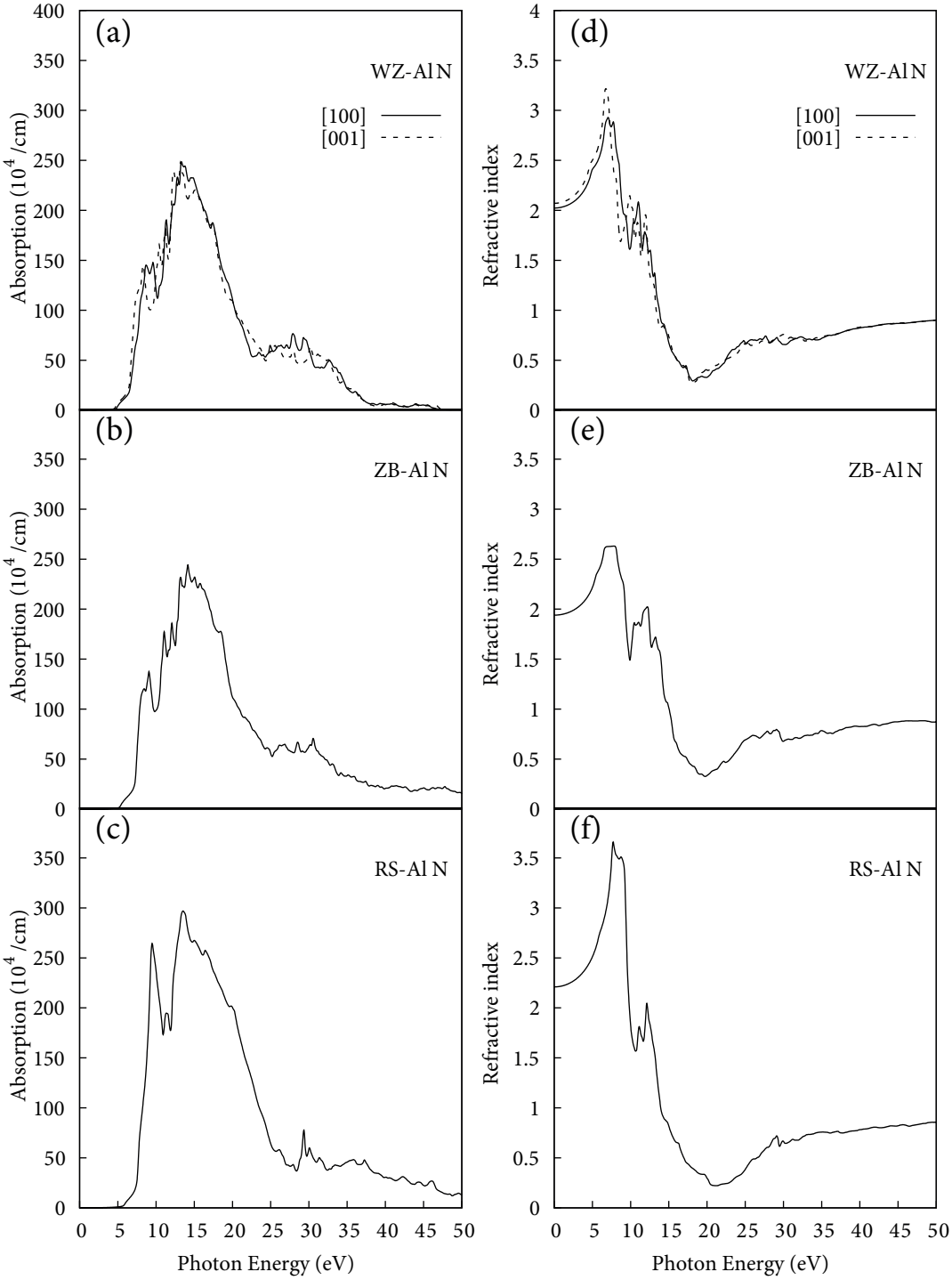

Figure 5. Adsorption function and refractive index calculated by PW-EV-GGA for WZ-AlN (a, d), ZB-AlN (b, e), and RS-AlN (c, f), respectively.

the available experimental and theoretical ones reported by high-cost calculations (LDA+QP, ASA-LDA+SX) in the literature. Hence, MBJP is decided to be the most accurate scheme among other approximations of this work for electronic band structure calculations of aluminum nitride phases.

References

[1] Perry, P. B.; Rutz, R. F. *Appl. Phys. Lett.* **1978**, *33*, 319-320.

[2] Li, J.; Nam, K. B.; Nakarmi, M. L.; Liu, J. Y.; Jiang, H. X.; Carrier, P.; Wei, S. H. *Appl. Phys. Lett.* **2003**, *83*, 5163-5165.

[3] Thompson, M. P.; Auner, G. W.; Zheleva, T. S.; Jones, K. A.; Simko, S. J.; Hilfiker, J. N. *J. Appl. Phys.* **2001**, *89*, 3331-3336.

[4] Edgar, J. H., Ed. *Properties of Group III Nitrides*; INSPEC: London, UK, 1994.

[5] Van de Walle, C. G. In *7th Trieste Semi-Conductors Symposium: Wide Band Gap Semiconductors*, Trieste, Italy, 8–11 June 1992.

[6] Fiorentini, V.; Methfessel, M.; Scheffler, M. *Phys. Rev. B* **1993**, *47*, 13353-13362.

[7] Vurgaftman, I.; Meyer, J. R. *J. Appl. Phys.* **2001**, *89*, 5815-5875.

[8] Sang, L.; Liao, M.; Ikeda, N.; Koide, Y.; Sumiya, M. *Appl. Phys. Lett.* **2011**, *99*, 161109-161112.

[9] Bablu, K. G.; Saiful, S. M. Z.; Ismail, S. In *Proceedings of the 5th International Conference on Development, Energy, Environment, Economics: Recent Advances in Energy*, Florence, Italy, 22–24 November 2014.

[10] Krugel, G.; Sharma, A.; Moldovan, A.; Wolke, W.; Rentsch, J.; Preu, R. In *39th IEEE Photovoltaic Specialists Conference*, Tampa, Florida, USA, 16–21 June 2013. New York, NY, USA: IEEE, p. 1249.

[11] Shultz, H.; Thiemann, K. H. *Solid State Commun.* **1977**, *23*, 815-819.

[12] Iwama, S.; Hayakawa, K.; Arizumi, T. *J. Crystal Growth* **1982**, *56*, 265-269.

[13] Petrov, I.; Mojab, E.; Powell, R. C.; Greene, J. E.; Hutman, L.; Sudgren, J. E. *Appl. Phys. Lett.* **1992**, *60*, 2491-2493.

[14] Ueno, M.; Onodera, A.; Shimomura, O.; Takemura, K. *Phys. Rev. B* **1992**, *45*, 10123-10126.

[15] Okumura, H.; Hamaguchi, H.; Koizumi, T.; Balakrishnan, K.; Ishida, Y.; Arita, M.; Chichibu, S.; Nakanishi, H.; Nagatomo, T.; Yoshida, S. *J. Crystal Growth* **1998**, *189*, 390-394.

[16] Uehara, S.; Masamoto, T.; Onodera, A.; Ueno, M.; Shimomura, O.; Takemura, K. *J. Phys. Chem. Solids* **1977**, *58*, 2093-2099.

[17] Vollstadt, H.; Ito, E.; Akaishi, M.; Akimoto, S.; Fukunaga, O. *Proc. Jpn. Acad. B* **1990**, *66*, 7-9.

[18] Xia, Q.; Xia, H.; Ruoff, A. L. *J. Appl. Phys.* **1993**, *73*, 8198-8200.

[19] Van Camp, P. E.; Van Doren, V. E.; Devreese, J. T. *Solid State Commun.* **1992**, *81*, 23-26.

[20] Rubio, A.; Corkill, J. L.; Cohen, M. L.; Shirley, E. L.; Louie, S. G. *Phys. Rev. B* **1993**, *48*, 11810-11816.

[21] Wright, A. F.; Nelson, J. S. *Phys. Rev. B* **1995**, *51*, 7866-7869.

[22] Satta, A.; Fiorentini, V.; Bosin, A.; Meloni, F. In *MRS Symposia Proceedings: Gallium Nitride and Related Materials*; Dupuis, R. D.; Edmond, J. A.; Ponce, F. A.; Nakamura, S., Eds.; Materials Research Society: Pittsburgh, PA, USA, 1996, p. 515.

[23] Buongiorno Nardelli, M.; Rapcewicz, K.; Briggs, E. L.; Bungaro, C.; Bernholc, J. In *MRS Symposia Proceedings: III-V Nitrides*; Ponce, F. A.; Moustakas, T. D.; Akasaki, I; Monemar, B. A., Eds.; Materials Research Society: Pittsburgh, PA, USA, 1997, p. 893.

[24] van Schilfgaarde, M.; Sher, A.; Chen, A. B. *J. Crystal Growth* **1997**, *178*, 8-31.

[25] Stamp, C.; Van de Walle, C. G. *Phys. Rev. B* **1999**, *59*, 5521-5535.

[26] Armenta, M. G. M.; Reyes-Serrato, A.; Borja, M. A. *Phys. Rev. B* **2000**, *62*, 4890-4898.

[27] Ferreira da Silvaa, A.; Dantasa, N. S.; de Almeidad, J. S.; Ahuja, R.; Persson, C. *J. Crystal Growth* **2005**, *281*, 151-160.

[28] Feng, W.; Cui, S.; Hu, H.; Zhao, W.; Gong, Z. *Physica B* **2010**, *405*, 555-558.

[29] Jiao, Z. Y.; Ma, S. H.; Yang, J. F. *Solid State Sci.* **2010**, *13*, 331-336.

[30] Çifçi, Y. Ö.; Çolakoğlu, K.; Deligöz, E. *Phys. Status Solidi C* **2007**, *4*, 234-237.

[31] Lambrecht, W. R. L.; Segall, B. *Phys. Rev. B* **1991**, *43*, 7070-7085.

[32] Wang, A. J.; Shang, S. L.; Du, Y.; Kong, Y.; Zhang, L. J.; Chen, L.; Zhao, D. D.; Liu, Z. K. *Comp. Mater Sci.* **2010**, *48*, 705-709.

[33] Bağcı, S.; Duman, S.; Tütüncü, H. M.; Srivastava, G. P. *Diam. Relat. Mater.* **2009**, *18*, 1057-1060.

[34] Tran, F.; Blaha, P. *Phys. Rev. Lett.* **2009**, *102*, 226401.

[35] Camargo-Martínez, J. A.; Baquero, R. *Phys. Rev. B* **2012**, *86*, 195106.

[36] Karch, K.; Bechstedt, F. *Phys. Rev. B* **1997**, *56*, 7404-7415.

[37] Gavrilenko, V. I.; Wu, R.Q. *Phys. Rev. B* **2000**, *61*, 2632-2642.

[38] Blaha, P.; Schwarz, K.; Madsen, G. K. H.; Kvasnicka, D.; Luitz, J. *WIEN2k, An Augmented-Plane-Wave + Local Orbitals Program for Calculating Crystal Properties*; Vienna University of Technology: Vienna, Austria, 2001.

[39] Mohammad, R.; Katırcıoğlu, Ş. *Indian J. Phys.* **2014**, *88*, 1021-1029.

[40] Perdew, J. P.; Wang, Y. *Phys. Rev. B* **1992**, *45*, 13244-13249.

[41] Engel, E.; Vosko, S. H. *Phys. Rev. B* **1993**, *47*, 13164-13174.

[42] Perdew, J. P.; Wang, Y. *Phys. Rev. B* **1986**, *33*, 8800-8802.

[43] Perdew, J. P.; Burke, S.; Ernzerhof , M. *Phys. Rev. Lett.* **1996**, *77*, 3865-3868.

[44] Becke, A. D.; Johnson, E. R. *J. Chem. Phys.* **2006**, *124*, 221101-221104.

[45] Edgar, J. H. *Properties of Group-III Nitrides*; IEE: London, UK, 1994.

[46] Suzuki, M.; Uenoyama, T.; Yanase, A. *Phys. Rev. B* **1995**, *52*, 8132-8139.

[47] Pugh, S. K.; Dugdale, D. J.; Brand, S.; Abram, R. A. *Semicond. Sci. Tech.* **1999**, *14*, 23-31.

[48] Goanoa, M.; Bellotti, E.; Ghillino, E.; Ghione, G.; Brennan, K. F. *J. Appl. Phys.* **2000**, *88*, 6467-6475.

[49] Persson, C.; Ferreira da Silva, A.; Ahuja, R.; Johansson, B. *J. Crystal Growth* **2001**, *231*, 397-406.

[50] Rezaei, B.; Asgari, A.; Kala, M. *Physica B* **2006**, *371*, 107-111.

[51] Akasaki, L.; Hashimoto, M. *Solid State Commun.* **1967**, *5*, 851-853.